Received: 15 January 2020 | Revised: 31 October 2020 | Accepted: 18 November 2020

DOI: 10.1002/we.2598

WILEY

RESEARCH ARTICLE

A full three-dimensional model for the estimation of the natural frequencies of an offshore wind turbine in sand

Philip Alkhoury | Abdul-Hamid Soubra | Valentine Rey | Mourad Aït-Ahmed

University of Nantes, France

Correspondence
Philip Alkhoury and Abdul-Hamid Soubra, University of Nantes, France.
Email: philip.alkhoury@etu.univ-nantes.fr, Abed.Soubra@univ-nantes.fr

Funding information
Communauté d'Agglomération de la Région Nazairienne et de l'Estuaire; WEAMEC

Abstract

The design of an offshore wind turbine (OWT) founded on a monopile foundation is principally based on dimensioning criteria related to its fundamental frequencies. These frequencies must remain outside the excitation frequencies to avoid resonance. For the calculation of the OWT natural frequencies, several studies exist, but few of them simultaneously consider both the real geometrical configuration of the OWT superstructure (tower, blades, and transition piece) and the three-dimensional (3D) soil domain and its interaction with the monopile foundation. This paper aims at filling this gap. A rigorous 3D finite element method-based model of a 10 MW DTU OWT installed in sand is developed. The aim is to perform a structural modal analysis of the wind turbine in parked condition. The obtained natural frequencies are compared with those corresponding to other simplified models available in literature for the foundation and the superstructure in the scope of giving an insight about how poorly the existing simplified models can predict the OWT natural frequencies. Finally, a parametric analysis is performed to study the effect of the water depth, the monopile dimensions (diameter, thickness, and embedded depth), the transition piece height, and the sandy soil relative density on the system natural frequencies.

KEYWORDS

foundation models, monopile, natural frequency, offshore wind turbine, sand, superstructure models

1 | INTRODUCTION

Offshore wind is considered as one of the most cost-effective means of reducing society dependence on fossil fuels. Exploitation of offshore wind energy from a severe environment like the sea requires resistant offshore wind turbines (OWTs) with suitable foundations. This paper focuses on the study of a multi-megawatt OWT founded on a large-diameter monopile in sand.

During their lifetime, OWTs are exposed to intense dynamic loading in a wide frequency range, which makes them dynamically sensitive structures. Therefore, tuning the natural frequencies of the whole structure is crucial during the design stage. Indeed, the first natural frequency of the overall wind turbine (denoted by f) should be carefully adjusted in a very narrow range to be outside the excitation frequencies and thus to avoid resonance.

The excitation sources on OWTs arise from the wind turbulence, the ocean waves, the rotational speed of the rotor (denoted by 1P), and the vibrations caused by the blades passing in front of the tower, causing a shadowing effect (termed as 2P/3P depending on the number of blades).

The 1*P* frequency is not a single frequency but a frequency range bounded by the lowest and highest speeds of the rotor. This is due to the fact that almost all modern industrial wind turbines are equipped with variable speed rotors. Both wind and wave frequencies are typically below the 1P frequency, but they can cover a relatively wide frequency spectrum. In order to ensure that no resonance occurs, three options can be considered in the design phase:

i. "Soft-soft design (i.e. $f < 1P$ *range*)," which yields a very flexible structure for OWTs.
ii. "Soft-stiff design (i.e. $1P$ *range* $< f < 3P$ *range*)." This is the most common in the current offshore development.
iii. "Stiff-stiff design (i.e. $f > 3P$ *range*)." This design requires very stiff support structure.

Stiff-stiff design appears as the safest solution. However, this would require massive support structures and foundations involving higher costs of materials, transportation, and installation. Thus, from an economic point of view, softer structures are desirable. It is not surprising that almost all of the installed wind turbines are based on soft-stiff designs.

As it will be shown in the next section, the determination of the natural frequencies of a monopile-supported OWT is generally performed in literature based on simplifying assumptions related to the soil-foundation interaction and/or the superstructure. In most previous works, the soil and the foundation are replaced by coupled/uncoupled springs at mudline, distributed springs along the monopile, or *via* a simplified model based on the apparent fixity approach. Also, the superstructure is usually modeled using simplified assumptions employing beam elements for the monopile and the tower and a lumped mass for the rotor-nacelle assembly (RNA). The accuracy of the above-mentioned simplifying assumptions is thus questionable.

One of the main objectives of this paper is to construct a rigorous three-dimensional (3D) finite element method FEM-based model that explicitly considers the entire soil-foundation-structure system and that can be used for natural frequencies characterization. The interactions between the superstructure, the foundation, and the soil may have a significant influence on the natural frequencies. A rigorous modeling of the three components (soil, foundation, and superstructure) with their corresponding geometrical and mechanical properties together with a rigorous modeling of the interactions between these components is thus necessary. The other objective of the paper is to check the accuracy of the currently used simplified assumptions for the soil-foundation system as well as for the superstructure by comparing the results of the OWT natural frequencies based on these assumptions with those provided by the developed 3D FEM-based model. This allows one to give an insight about how poorly the existing simplified models can predict the OWT natural frequencies. Another objective of the work is to tune the mostly used simplified foundation models, making use of the developed 3D FEM-based model. A final objective of this work is to employ the developed 3D FEM-based model to determine the effect of the different parameters of the soil and the foundation on the first natural frequency, the existing simplified models being unable to explicitly include the soil, and foundation design parameters.

In the present study, a full 3D FEM-based model of the 10 MW DTU wind turbine is developed using the commercially available finite element (FE) code Abaqus/Standard. The geometrical properties of the wind turbine components (blades, tower, transition piece, and monopile) are explicitly considered, and the soil is modeled as a 3D continuum. A modal analysis based on the developed 3D model is carried out to calculate the natural frequencies of the 10 MW DTU OWT in parked condition. The suitability of the different simplified models usually employed in literature for the superstructure and the soil-foundation system is investigated and discussed. In addition, the effect of several parameters related to the soil-foundation system (such as the soil stiffness, the monopile geometrical properties, and the transition piece height) on the OWT first natural frequency is presented and discussed.

The paper is organized as follows: a literature review on the modeling of an OWT system is presented in Section 2. The description of the DTU 10 MW reference wind turbine and the development of the corresponding 3D model and its resolution with FEM using Abaqus software are presented in Section 3. Section 4 presents the numerical results and a comparative study with other simplified models available in literature. A parametric study is presented and discussed in Section 5. Some concluding remarks are provided in Section 6.

2 | LITERATURE REVIEW ON THE MODELING OF OWT

This section presents an overview on the different models available in literature for the OWT structural components and the interaction of the foundation with the surrounding soil.

The fixed-base model is the simplest way to model the soil-foundation interaction of OWTs. This model ignores completely the flexibility of the soil and assumes a perfectly rigid connection of the turbine support structure at seabed. Zaaijer[1] analyzed four different modeling techniques of the soil-foundation system to assess the first and second natural frequencies of a monopile-supported OWT while introducing the soil flexibility. The first model is the apparent fixity model in which the true pile foundation and the surrounding soil medium are replaced by an equivalent cylindrical pile (with new stiffness and length) that is fully fixed at its base. The second model is the distributed spring model (or the Winkler model). It considers the true length of the pile and replaces the soil with elastic springs distributed along the embedded pile length. The third model is the stiffness matrix model in which both the soil and the embedded pile are completely replaced by a stiffness matrix assigned to the

bottom of the OWT located at the seabed level. This model includes three springs (lateral, rotational, and cross-coupling springs). It is known as the coupled spring model. Finally, the fourth model is the uncoupled spring model where the soil and embedded pile are substituted by only two independent springs (i.e. lateral and rotational springs) placed at the seabed level. We present hereafter a review of the different foundation modeling techniques used in literature for the computation of the natural frequencies of a monopile-supported OWT. These models include the fixed-base model, the Winkler model, the coupled/uncoupled spring model, the apparent fixity model, and the FEM-based model.

Bazeos et al.[2] and Lavassas et al.[3] adopted the fixed-base model. In their studies, the OWT is modeled by beam/shell elements for the tower and a lumped mass for the RNA. In this model, the foundation and the surrounding soil are completely neglected. Similarly, Asareh et al.[4] adopted the fixed-base model. In their work, the OWT is modeled using shell elements for the tower, elastic beam elements for the blades, and a point mass for the nacelle-hub assembly.

The well-known Winkler[5] model has successfully been employed for offshore structures related to oil and gas for many years due to its simplicity and efficiency. In this approach, the pile is replaced by an elastic beam and the soil by a set of independent springs distributed along the monopile embedded depth. For the computation of the natural frequencies of an OWT, the spring stiffness at a given depth is usually determined by the initial slope of the so-called $p - y$ curves. The $p - y$ curves used in practice are those recommended by American Petroleum Institute (API).[6] The API $p - y$ curves for piles in sand are given as follows:

$$p = A.p_u.tanh\left[\frac{k.z}{A.p_u}.y\right], \tag{1}$$

where p_u is the ultimate lateral resistance at depth z below the mudline, k is the rate of increase with depth of the initial modulus of subgrade reaction, A is an empirical factor accounting for static or cyclic external loading condition, and y is the lateral deflection at depth z. The values of k and p_u are specified in the API design code as a function of the friction angle of the sand. It is worth mentioning that the widely used API model was initially calibrated against response of small-diameter slender piles (length to diameter ratio of 30–50) suitable for offshore fixed platform applications (oil and gas). However, for an OWT founded on a monopile, the length to diameter ratio of the monopile is between 4 and 8, thus giving the monopile of the OWT a rigid behavior. The API-based $p - y$ curves are thus not suitable for large-diameter monopiles.

Despite the limitations of the API-based $p - y$ curves, these curves have been used by various investigators (Andersen et al.,[7] Bisoi and Haldar,[8] Haldar et al.,[9] and Wang et al.[10]). Indeed, these authors modeled the soil-monopile system by a nonlinear Winkler approach and used the API-based $p - y$ curves to determine the spring stiffness distribution. In their studies, the OWT tower was merely modeled by a beam with a lumped mass at its top to represent the nacelle and the blades. Notice that Zuo et al.[11] also adopted the nonlinear Winkler approach with the API-based $p - y$ curves. Although the soil-structure interaction was not properly modeled by Zuo et al.[11] due to the limitation of the API-based $p - y$ curves for a large-diameter monopile, the OWT superstructure (tower and blades) was explicitly modeled within Abaqus using shell elements. Furthermore, the rotation of the blades with respect to the rotor was also simulated. Finally, the nacelle and the hub were modeled by a point mass lumped at the tower top. The soil-structure interaction (SSI) was found to have a predominant effect on the tower vibrations and a minimal effect on the in-plane vibrations of the blades.

Apart from the API-based $p - y$ curves, Prendergast et al.[12,13] used the modulus of subgrade reaction to derive the stiffness properties of the distributed springs used in the Winkler model for the computation of the first natural frequency under the effect of scour. In their studies, the OWT structure was simply modeled by a beam with a lumped mass at its top as a representation of the nacelle/blades system. Notice that the used modulus of subgrade reaction was the one derived by Ashford and Juirnarongrit,[14] which was originally developed by Vesic.[15] It is given as follows:

$$K = \frac{E_0}{1-\nu_0{}^2}\left[\frac{E_0 D^4}{E_P I_P}\right]^{1/12}, \tag{2}$$

where D, E_P, and I_P are respectively the diameter, the Young modulus, and the moment of inertia of the monopile; and E_0 and ν_0 are respectively the soil small-strain Young modulus and Poisson ratio. The individual spring stiffness at a given depth is obtained by multiplying the corresponding K value by the distance separating two consecutive springs. Another approach was used by Prendergast et al.[13] to derive the spring stiffness distribution in sand from $p - y$ curves based on cone penetration test (CPT) data making use of the expression proposed by Suryasentana and Lehane.[16] This expression is given as follows:

$$\frac{p}{\gamma.z.D} = 2.4\left(\frac{q_c}{\gamma.z}\right)^{0.67}\left(\frac{z}{D}\right)^{0.75}\left\{1-exp\left[-6.2\left(\frac{z}{D}\right)^{-1.2}\left(\frac{y}{D}\right)^{0.89}\right]\right\}, \tag{3}$$

where p is the soil reaction at a given depth z, q_c is the corresponding cone tip resistance, γ is the bulk unit weight of the soil, D is the monopile diameter, and y is the lateral deflection of the monopile at depth z.

The modeling of the soil-foundation system using the coupled/uncoupled spring models has received much attention in the literature. Adhikari and Bhattacharya[17] used two uncoupled springs (lateral and rotational springs) at mudline to represent the foundation. In their study, the OWT tower was modeled using the Euler-Bernoulli beam model with a mass at the tower top to represent the RNA. In Arany et al.,[18,19] the foundation was modeled by three coupled springs at mudline (lateral, rotational, and cross-coupling springs). In their study, they compared the effect of modeling the OWT tower using a Timoshenko beam model instead of using an Euler-Bernoulli beam model. The authors have found that the cross-coupling term in the stiffness matrix cannot be excluded and that the Timoshenko beam model does not improve the results significantly, and thus, the assumption of using the Euler-Bernoulli beam is sufficient when calculating the natural frequencies.

Notice that the stiffness properties of the coupled/uncoupled spring models are usually based on load–displacement curves. For instance, Jung et al.[20] computed the coupled spring stiffness properties based on load–displacement curves obtained from FE simulations. In their study, the structural components of the OWT were modeled by the beam flexible elements available in FAST.[21] Table 1[22–24] summarizes some of the expressions that may be used to calculate the stiffness of the coupled lateral and rotational springs (K_{HH}, K_{RR}, K_{RH}) in the case of a rigid monopile. These expressions correspond to a linear or a parabolic soil profile to capture the depth-dependent Young modulus usually observed in practice.

In addition to the distributed spring model and the coupled/uncoupled spring model, some researchers incorporated the influence of SSI in their work by modeling the foundation using the apparent fixity (AF) model (Abhinav and Saha[25] and Velarde et al.[26]). The AF model replaces the foundation and the soil by a fictitious cylinder fixed at its base below the mudline. The length, L_{AF}, and bending rigidity, EI_{AF}, of the fictive AF cylinder are determined such that the stiffness matrix of the AF cylinder (cf. last term of Equation 4) is identical to the stiffness matrix of the real soil-foundation system (cf. second term of Equation 4):

$$K = \begin{bmatrix} K_{HH} K_{HR} \\ K_{RH} K_{RR} \end{bmatrix} = \begin{bmatrix} \frac{12EI_{AF}}{L_{AF}^3} & -\frac{6EI_{AF}}{L_{AF}^2} \\ -\frac{6EI_{AF}}{L_{AF}^2} & \frac{4EI_{AF}}{L_{AF}} \end{bmatrix}. \quad (4)$$

The common practice in offshore geotechnical engineering is to match only the diagonal stiffness terms while neglecting the off-diagonal terms. This permits the calculation of the two parameters of the AF model (i.e. L_{AF} and EI_{AF}). Recently, Løken and Kaynia[27] developed a new method to improve the traditional AF model. The method proposed by these authors enables to consider all the terms of the stiffness matrix. This was done by replacing the single AF cylinder with two successive cylinders as it will be shown later in this paper. The new developed method by Løken and Kaynia[27] was known as the improved AF method.

Apart from the simplified models presented above and which are based on several assumptions for the soil-foundation system, the FEM (which explicitly considers the 3D soil continuum) was also used in literature to represent the soil-foundation interaction. This method allows complex foundation geometries to be modeled, and it can consider sophisticated constitutive laws for the soil. Also, soil-foundation separation, gap formation, and other interface nonlinearities can be included within this method.

The FEM has been used by various investigators for a rigorous modeling of the soil-monopile system. For instance, Achmus and Thieken[28] and Abdel-Rahman and Achmus[29] predicted the behavior of monopiles under combined horizontal and vertical loadings using a FEM-based model for the soil-monopile system. Prowell[30] also used the FEM for the soil-monopile system when calculating the natural frequencies of a 5 MW wind turbine. Jalbi and Bhattacharya[31] compared the value of the first natural frequency obtained using a 3D soil continuum with the one obtained from a simplified method developed at the University of Surrey. In their work, the RNA was merely modeled by a lumped mass located at the top of the beam element representing the turbine tower. In order to perform time-domain analysis in the presence of environmental loads, Corciulo et al.[32] developed a 3D hydro-mechanical model. This model was employed by Kementzetzidis et al.[33] to perform nonlinear time-domain simulations in order to predict the response of an 8 MW OWT subjected to a long loading history of approximately 2 h. The scope of their work was to investigate/explain the drops in natural frequency observed in the field during storms as well as its subsequent recovery. The same model was used by Kementzetzidis et al.[34] to study the influence of sand cyclic behavior on energy dissipation and resonance in OWTs. Finally, Ma et al.[35] used a 3D FEM-based model to investigate the performance of an OWT founded on a monopile in sand under long-term cyclic lateral loading, with particular attention to the effects of long-term cyclic loading on the deflection and rotation of the support structure under serviceability limit state (SLS) and ultimate limit state (ULS).

TABLE 1 Stiffness properties of the coupled springs as given by some authors

Authors	Soil model	K_{HH}	K_{RR}	K_{RH}
Poulos and Davis[22]	Linear[a]	$\frac{1}{2}L^2.n_h$	$\frac{1}{4}L^4.n_h$	$-\frac{1}{3}L^3.n_h$
Huggins and Basu[23]	Linear[b, c]	$\frac{4E_s.r}{f(\nu)}.\left(\frac{L}{D}\right)^{1.66}$	$\frac{15.4E_s.r^3}{f(\nu)}.\left(\frac{L}{D}\right)^{3.45}$	$-\frac{6.7E_s.r^2}{f(\nu)}.\left(\frac{L}{D}\right)^{2.6}$
Shadlou and Bhattacharya[24]	Parabolic[b, c]	$5.33E_s.r.f(\nu).\left(\frac{L}{D}\right)^{1.07}$	$13E_s.r^3.f(\nu).\left(\frac{L}{D}\right)^{3}$	$-7.2E_s.r^2.f(\nu).\left(\frac{L}{D}\right)^{2}$

[a]The coefficient of subgrade reaction n_h for sand is given as $n_h = \frac{A.\gamma_{sand}}{1.35}$, where γ_{sand} is the specific weight of sand and A = 100–300 for loose sand.
[b]Poisson ratio effects may be considered by the function $f(\nu)$ presented by Randolph: $f(\nu) = \frac{1+\nu}{1+0.75\nu}$.
[c]E_s is the soil Young modulus at a depth equal to the pile diameter. L, r, and D are the monopile embedded length, radius, and outer diameter, respectively.

As a conclusion, the existing models for an OWT are generally based on simplifying assumptions for the superstructure and/or the soil-foundation system. This paper aims at filling this gap by simultaneously considering both the real geometrical configuration of the superstructure (tower, blades and transition piece) and the 3D soil domain and its interaction with the foundation. The next section gives a description of the developed 3D FEM-based model for the DTU 10 MW reference turbine.

3 | MECHANICAL MODEL

3.1 | DTU 10 MW reference wind turbine

The modern DTU 10 MW three-bladed wind turbine is selected as an example application in the present work because its properties are well defined in many previous studies (cf. Bak et al.[36]). The turbine tower of 115.63 m height is divided into 10 sections with constant diameter and thickness within each section. The outer diameter and wall thickness decrease as passing from the bottom to the tower top. The outer diameter and wall thickness at the top and bottom of the tower are (5.5, 0.02 m) and (8.3, 0.038 m), respectively. The total length of the monopile is chosen as 80 m, in which 25 and 45 m are in the water and seabed, respectively, and another 10 m is added above the mean sea level corresponding to the transition piece. The diameter of the monopile foundation is taken the same as the bottom cross-section of the tower (i.e. 8.3 m). Notice that a monopile thickness of 0.09 m is chosen to respect the minimum wall thickness recommended by API[37] and given as follows:

$$t = 6.35 + \frac{D}{100}, \tag{5}$$

where t (mm) is the wall thickness of the monopile and D (mm) its outer diameter.

The radius of the hub is 2.8 m, and the blade length is 86.366 m. The distance from the hub center to the blade tip is therefore 89.166 m. The DTU blade is made up of five airfoil sections where their corresponding geometries can be found in Bak et al.[36] Figure 1 and Table 2 provide the main characteristics of the wind turbine.

3.2 | Development of the 3D FEM-based model

The 3D model of the DTU 10 MW wind turbine was developed in this paper using the FE code Abaqus. As natural frequency is concerned with very small amplitude vibrations, linear modal analysis is sufficient (cf. Letcher[38]). The deformation of the foundation will be small, and

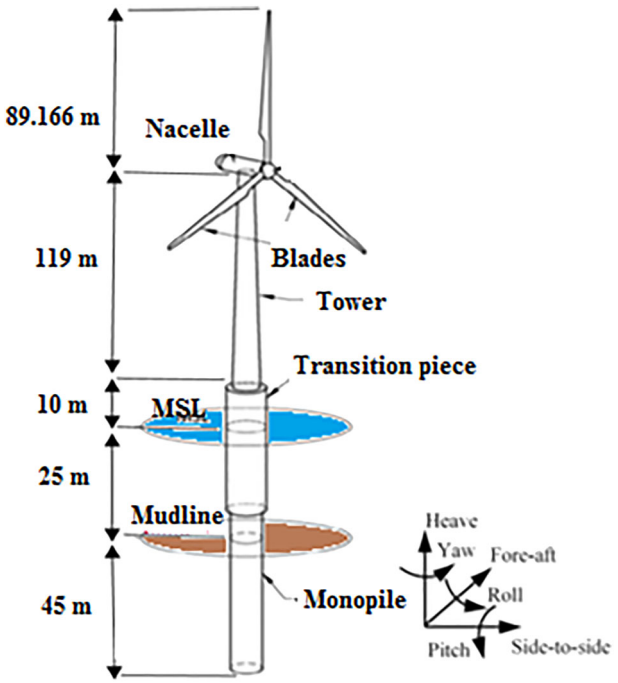

FIGURE 1 DTU 10 MW OWT (front view)

TABLE 2 Properties of DTU 10 MW wind turbine

DTU 10 MW wind turbine properties		
Basic description	Max. rated power	10 MW
Blade	Rotor orientation, configuration	Upwind, 3 blades
	Rotor diameter	178.332 m
	Hub height	119 m
	Cut-in, rated, cut-out wind speed	4, 11.4, 25 m/s
	Cut-in, rated rotor speed	6, 9.6 rpm
	Length	86.366 m
	Number of airfoils along blade length	5
	Overall mass	41,716 kg
Hub and nacelle	Hub diameter	5.6 m
	Hub mass	105,520 kg
	Nacelle mass	446,036 kg
Tower	Height	115.63 m
	Mass	682, 442 kg

consequently, the consideration of the initial foundation stiffness would suffice for this purpose. Practically speaking, the use of the small-strain properties of the soil is adopted in this paper for the linear modal analysis of the OWT. In this section, one presents the modeling of the different structural components and the soil-monopile system.

3.2.1 | Modeling of the OWT structural components

The 10 different parts of the tower as well as the 10 m transition piece above the mean sea water level were modeled using shell elements where 8-node layered shell elements S8R were employed. The monopile (in the sea water and in the soil medium) was modeled using solid elements, which enables one to conveniently consider the soil-monopile interaction. In order to ensure the connection between the 10 different tower parts, they were tied with each other at their adjacent cross-sections. A tied connection was also used for the two cross-sections that relate the transition piece to the tower and the monopile.

Steel S355 was used for the monopile, the tower, and the transition piece. It was assumed to follow an elastic isotropic behavior. Table 3 summarizes the material properties of the tower and the monopile. Note that the density of the tower and transition piece was increased by approximately 8% (ρ = 8,500 kg/m^3) in order to account for the mass of secondary structures (paints, welds, bolts, and flanges) that are not directly considered in the model (cf. Zuo et al.[11]). In the sea water, the vibrating monopile may induce acceleration to the surrounding sea water. The water-monopile interaction was modeled by the added mass method (e.g. Bi and Hao[39] and Zuo et al.[11]). Therefore, the effective density of the monopile in the sea water is 8,880 kg/m^3.

To consider the influence of the blades geometry on the response of the turbine, the blades were explicitly considered in the present 3D model. Because of the complex heterogeneous material of the blades, each blade was partitioned into 51 segments along its length where the number of segments corresponds to the data provided by Bak et al.[36] A generalized beam cross-section in Abaqus was defined for every segment, and each cross-section was assigned the stiffness properties that can be found in Bak et al.[36] These properties include (i) the cross-sectional area, (ii) the shear stiffness along the two axes (flapwise and edgewise directions), (iii) the bending stiffness along the two axes (flapwise and edgewise directions), the extensional and torsional stiffnesses, and (iv) the positions of the mass and shear centers. Note that the orientation of the blade beams was modified so that the strong axis of the blade is alongside the edgewise direction of the blade (cf. Letcher[38] and Asareh et al.[4]). Note also that the mass of the blade was given as a constant mass over each structural section along the entire blade length.

TABLE 3 Material properties of the wind turbine

Component	Material	Density (kg/m^3)	Young modulus (GPa)	Poisson ratio
Tower + transition piece	Steel	8,500	210	0.3
Monopile in the water	Steel	8,880	210	0.3
Monopile in the soil	Steel	7,850	210	0.3

The nacelle/hub assembly was considered as a lumped mass placed at a reference point (RP) whose position coincides with the nacelle center of mass defined in the turbine specifications (cf. Bak et al.[36]). Only the mass and rotary inertia of the assembly were considered. The nodes of the tower top cross-section were coupled with the nacelle/hub RP to simulate the interconnection between them. In order to simulate the rotation of the blades with respect to the tower (which can be used in further dynamic analysis), a hinge connection between the nacelle/hub RP and the rotor was used. In this way, the rotor can freely rotate in the axis of rotation relative to the drive shaft of the turbine. Notice that the drive shaft was not considered throughout the analysis. In addition, the rotation of the blades was not explicitly considered in the modal analysis by using Abaqus and thus only the parked condition was studied in this paper.

Figure 2A shows the 3D model of the wind turbine superstructure, and Figure 2B shows the blade which has been modeled using the concept of generalized beam cross-section.

3.2.2 | Modeling of the soil-monopile system

The interaction between the monopile foundation and the surrounding soil may significantly influence the natural frequency of an OWT. A 3D soil domain having a diameter 20D and a height of 1.7L was adopted (see Figure 3), where D is the monopile outer diameter and L is its corresponding embedded depth in the soil. The lateral boundary of the 3D soil domain was restrained in the horizontal direction; however, the base of this domain was fixed in all directions. The soil around and inside the monopile was modeled by a weightless linear elastic material using 8-noded brick elements with reduced integration and hourglass control. Concerning the monopile-soil interface, it was modeled using the small sliding, surface-to-surface, and master/slave contact pair formulation described in Abaqus. The penalty contact method with small sliding was utilized to simulate the tangential and normal contact behavior between the monopile and the soil. In the tangential direction, a friction coefficient of 0.4–0.48 was used depending on the sand type (cf. Gentils et al.[40]). Figure 3 shows the full 3D model of the wind turbine including the soil domain and the corresponding mesh.

Small-strain soil elastic properties

As mentioned before, the soil deformation may be conveniently assumed to be small in this paper because we are considering the initial stiffness of the soil-foundation system. The OWT response is thus governed by the properties of the soil in the small-strain regime where the soil strain is below 10^{-3} (cf. CFMS[41]). In this small-strain regime, the soil behavior may be assumed to be linear elastic, and the corresponding elastic properties are referred to herein as small-strain elastic properties.

The initial tangent (small-strain) shear modulus (G_0) is an important parameter for the natural frequency calculation. It depends mainly on the vertical effective stress, and hence, it increases with depth. Throughout the literature, there exists different empirical equations that describe the

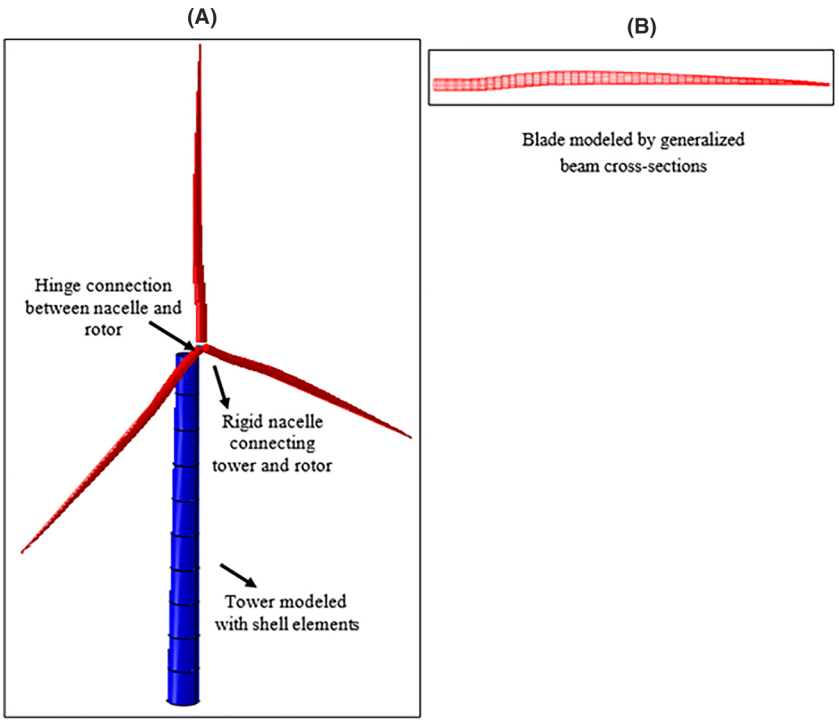

FIGURE 2 3D model of (A) the wind turbine components (the monopile and soil medium are not shown) and (B) the blade

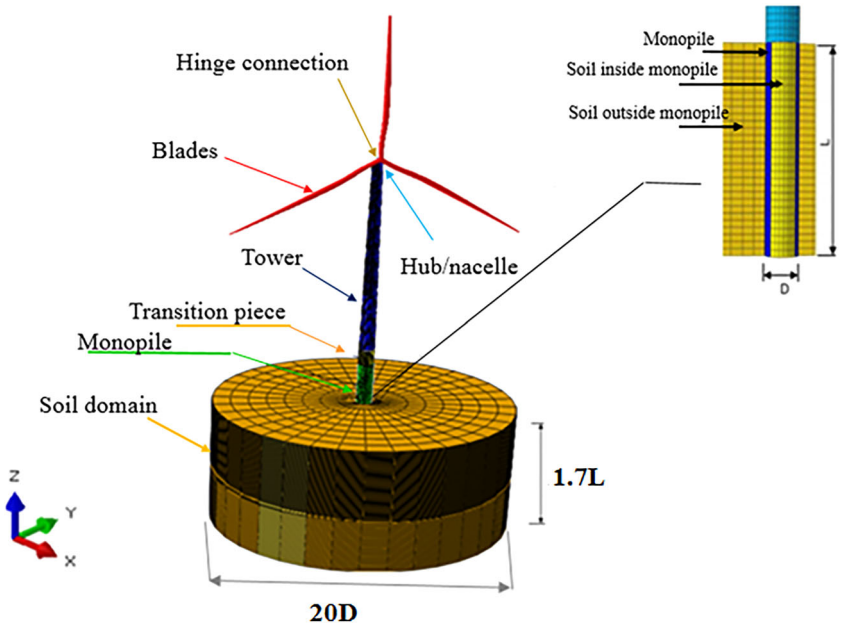

FIGURE 3 3D model of the wind turbine taking into account the soil-structure interaction

variation of G_0 with depth for a sandy soil (cf. Hardin and Black,[42] Seed and Idriss,[43] Hardin and Drnevich,[44] Jardine,[45] and Oztoprak and Bolton[46]). In the present work, a sandy soil profile with depth-dependent small-strain shear modulus was considered based on the expression given by Jardine[45] and used by Prendergast et al.[12] The G_0 profile suggested by Jardine[45] depends on the cone tip resistance (q_c) values, as follows:

$$G_0 = q_c\left[A + B\eta - C\eta^2\right]^{-1}, \tag{6}$$

where A = 0.0203, B = 0.00125, $C = 1.216 \times 10^{-6}$, and $\eta = q_c(P_a\sigma_v')^{-0.5}$; P_a is a reference pressure of 100 kPa (atmospheric pressure), and σ_v' is the vertical effective stress (kPa). The CPT-based G_0 profile given by Equation 6 grants the possibility to consider a wide range of sands that are typically encountered in the offshore environment based on measured q_c values. In our work, synthetic CPT profiles derived by Lunne and Christopherson[47] and used by Prendergast et al.[12] were used. They are given by the following equation:

$$q_c = 60(\sigma_v')^{0.7}\exp(2.91D_r), \tag{7}$$

where D_r is the relative density of sand. The profile of the small-strain Young modulus E_0 was derived from the G_0 profile using the following equation:

$$E_0 = 2G_0(1+\nu_0), \tag{8}$$

where ν_0 is the small-strain Poisson ratio. The small-strain Poisson ratio adopted in this study was derived from the G_0 profile based on the relation proposed by Gu et al.[48] as follows:

$$\nu_0 = 0.62(G_0)^{-0.2}. \tag{9}$$

Figure 4A–D shows respectively the derived synthetic cone tip resistance (q_c) profile, the corresponding small-strain shear modulus (G_0) profile, the small-strain Poisson ratio (ν_0) profile, and the small-strain Young modulus (E_0) profile in the cases of loose, medium dense, and very dense sands having respectively a relative density of 30%, 50%, and 80% and corresponding bulk unit weights of 16, 18, and 20 kN/m^3.

4 | NUMERICAL RESULTS

For the estimation of the natural frequencies of the developed 3D model, a structural modal analysis was carried out using Abaqus/Standard. In the first subsection, one presents a comparison between the results of the developed 3D model (but considering a fixed tower base, i.e. with no

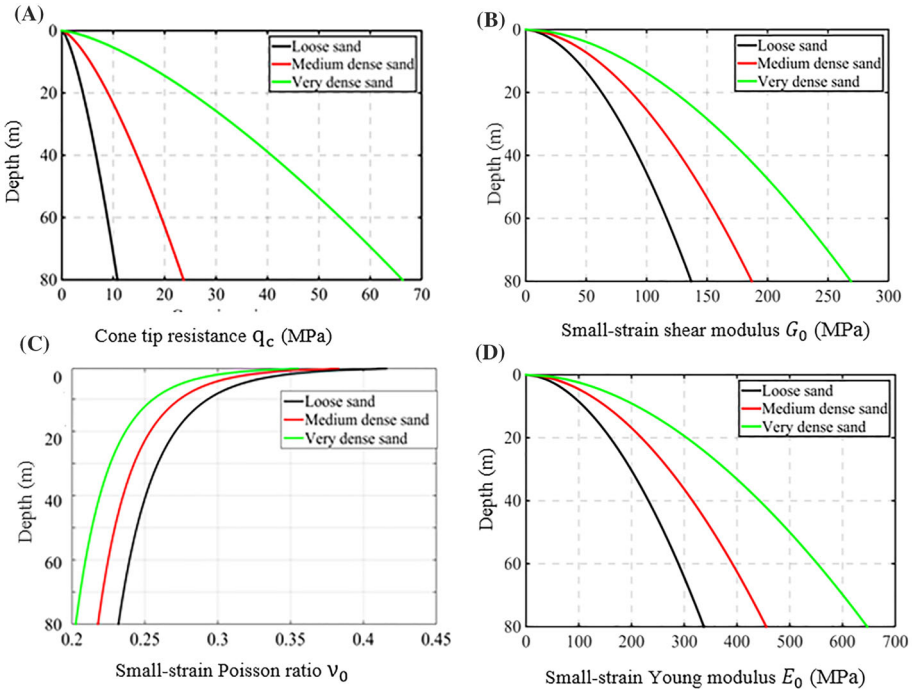

FIGURE 4 Synthetic sand profiles for loose, medium dense, and very dense sands. (A) Cone tip resistance q_c. (B) Small-strain shear modulus G_0. (C) Small-strain Poisson ratio ν_0. (D) Small-strain Young modulus E_0

SSI) and those of another study using HAWC2 simulator (for which a fixed base is imposed) to validate the mass and stiffness distribution considered in the analysis. Then, the results of the natural frequencies and the corresponding vibration modes of the 10 MW DTU OWT installed in a loose sand and incorporating the SSI are presented and discussed. Finally, the suitability of the different simplified foundation and superstructure models used in literature is investigated and discussed.

4.1 | Comparison with HAWC2 simulator

To validate the mass and stiffness distributions considered for the different components (tower, blades, nacelle, and hub) of the 3D developed model, the natural frequencies and the corresponding vibration modes are calculated for the 3D model and compared in Table 4 with those of a previous study by Bak et al.[36] using the aero-elastic servo simulator HAWC2 (cf. Larsen and Hansen[49]). From Table 4, it can be seen that the results show a very good agreement between the 3D developed model and the multibody dynamic model developed within HAWC2 simulator.

TABLE 4 Natural frequencies of the DTU 10 MW wind turbine computed in the case of a fixed-base tower

		First natural frequency (Hz)		
Mode	Description	HAWC2	Current study	Relative difference (%)
1	1st bending tower, side-side	0.249	0.250	0.4
2	1st bending tower, fore-aft	0.251	0.251	0
3	1st blade asymmetric, flapwise yaw	0.547	0.549	0.4
4	1st blade asymmetric, flapwise tilt	0.590	0.594	0.7
5	1st blade collective flap	0.634	0.626	−1.3
6	1st blade asymmetric, edgewise 1	0.922	0.933	1.2
7	1st blade asymmetric, edgewise 2	0.936	0.945	1
8	2nd blade asymmetric, flapwise yaw	1.376	1.391	1.1
9	2nd blade asymmetric, flapwise tilt	1.550	1.579	1.9
10	2nd blade collective flap	1.763	1.740	−1.3
11	2nd bending tower, side-side	1.969	2.108	7.1
12	2nd bending tower, fore-aft	2.247	2.301	2.4

4.2 | Results of the 3D FEM-based model

Table 5 and Figure 5 provide the computed natural frequencies and the corresponding vibration modes of the wind turbine installed in loose sand as obtained from a modal analysis in Abaqus/Standard using the present 3D model. The modal analysis shows that the major mode shapes of a monopile-supported OWT are the first bending modes of the tower in the side-side and the fore-aft directions. The natural frequencies of these two modes are different because the moment of inertia of the RNA in the roll motion is different from that corresponding to the pitch motion. Notice however that the difference is very small because the tower and foundation have axial symmetric shapes and properties. The subsequent mode shapes are those of the rotor (Modes 3, 4, 5, 6, 7, 9, 11, and 12) and the second bending modes of the tower (Modes 8 and 10).

It should be mentioned that the values of the natural frequencies obtained so far correspond to a simplified modeling of the transition piece (cf. Figure 6A). Indeed, the transition piece was considered to have the same diameter as the tower and the monopile. In order to check the validity of this simplified modeling, a more refined modeling of the connection between the tower base, the transition piece, and the monopile was considered herein (cf. Figure 6B), where the annulus between the monopile and the transition piece was filled with an ultra high performance grout made of Ducorit D4® (cf. Densit[50]). The transition piece was modeled using shell elements as was the case of the continuous connection presented in Figure 6A. The grout connection of density 2,740 kg/m^3 was modeled using 20-noded brick elements with reduced integration C3D20R. It was assumed to follow a linear elastic material with a Young modulus of 70 GPa and a Poisson ratio of 0.19. The first natural

TABLE 5 Natural frequencies of the monopile-supported 10 MW DTU wind turbine installed in a loose sand as computed by the present 3D model

Mode	Description	Frequency (Hz)
1	1st bending tower, side-side	0.201
2	1st bending tower, fore-aft	0.202
3	1st blade asymmetric, flapwise yaw	0.544
4	1st blade asymmetric, flapwise tilt	0.589
5	1st blade collective flap	0.623
6	1st blade asymmetric, edgewise 1	0.932
7	1st blade asymmetric, edgewise 2	0.941
8	2nd bending tower, fore-aft	1.297
9	2nd blade asymmetric, flapwise yaw	1.370
10	2nd bending tower, side-side	1.460
11	2nd blade asymmetric, flapwise tilt	1.701
12	2nd blade collective flap	1.762

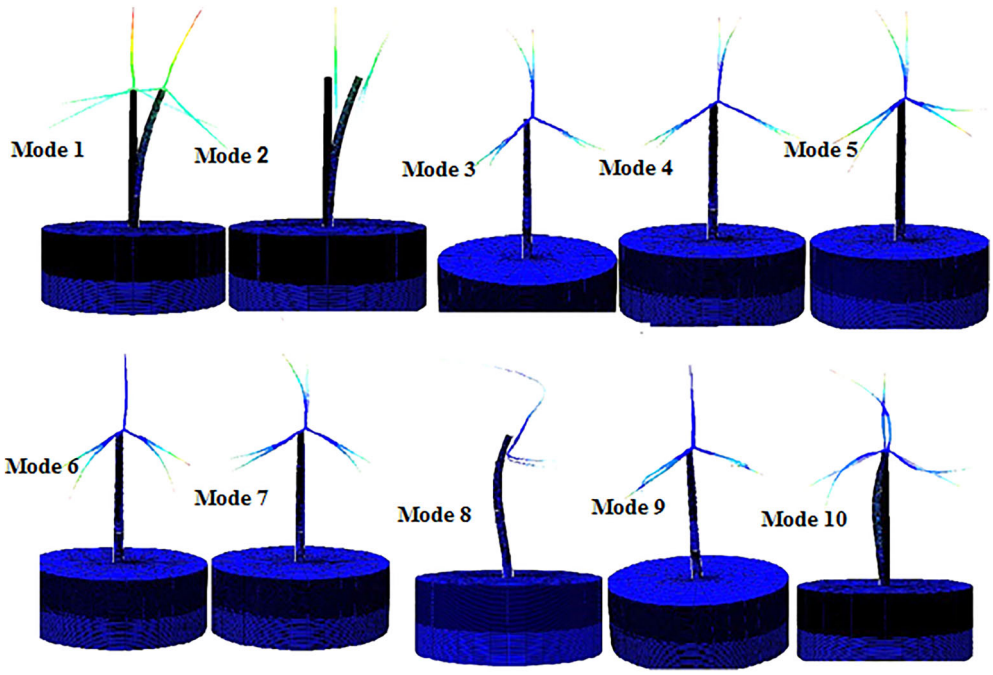

FIGURE 5 Vibration modes of the wind turbine

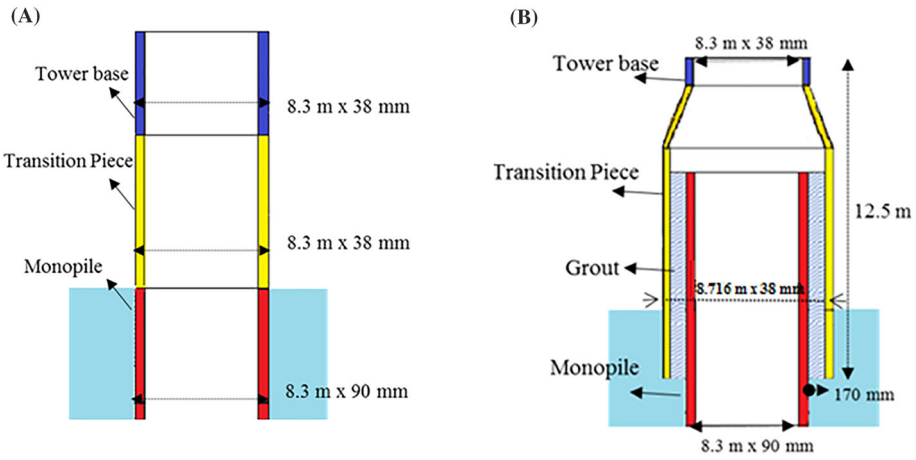

FIGURE 6 Representation of the connection between the tower base, the transition piece, and the monopile. (A) Continuous connection. (B) Grouted connection

frequency was found to be 0.200 Hz in the case of a grouted connection and 0.201 Hz in the absence of the grout (i.e. a percentage difference of 0.3%). Thus, the assumption of using a continuous connection between the tower base, the transition piece, and the monopile is acceptable and can be used throughout the paper.

4.3 | Comparison with other simplified models

To the knowledge of the authors, there is no publication so far that gives a well-structured comparison and estimation of the deviations obtained upon calculating the natural frequencies of an OWT when using the different simplified models for the soil-foundation system and the superstructure. Notice that the estimation of the deviations should be done by comparing the values of the natural frequencies provided by the simplified models with those obtained using a rigorous 3D FEM-based model.

It should be noted that a comparison between different simplified foundation models has been done so far by Zaaijer[1] and Jalbi and Bhattacharya[31] to a very limited extent. In Zaaijer,[1] the reference model (Winkler distributed spring model) used for the comparison was itself a simplified model because of its unsuitability for large-diameter monopiles, and thus, the comparison cannot serve as a reliable reference. Concerning the comparison performed by Jalbi and Bhattacharya,[31] although the reference model was based on a 3D soil domain, the comparison is somehow limited because it mainly focused on a simplified method developed by their research group at the University of Surrey.

In order to test the suitability of the different simplified models used in literature for the foundation and the superstructure, the corresponding natural frequencies were calculated using Abaqus and compared with those provided by the 3D model in the case of a loose sand.

4.3.1 | Foundation models

The alternative foundation models used for the comparison are the fixed-base model, the coupled spring model, the apparent fixity model, and the distributed spring model, as illustrated in Figure 7. For all these models, the same superstructure model used in the 3D developed model was adopted.

The fixed-base model is considered in this section to show the importance of taking into account the soil-structure interaction when calculating the natural frequencies of the OWT. The coupled spring model makes use of the stiffness values provided by Poulos and Davis,[22] Huggins and Basu,[23] and Shadlou and Bhattacharya[24] where the corresponding formulas are given in Table 1. The corresponding numerical values are given in Table 6, where the constant A is taken equal to 200 for loose sand in the expression given by Poulos and Davis.[22]

Concerning the apparent fixity model, two different approaches are considered in this study. The first one is the traditional AF approach. This approach considers a single cylinder whose properties (length L_{AF} and flexural rigidity EI_{AF}) were determined from the diagonal terms of the stiffness matrix as given in Equation 4. The second one is the improved AF approach proposed by Løken and Kaynia,[27] which considers two consecutive cylinders as shown in Figure 8. The parameters (length and rigidity) of the two cylinders can be determined from both the diagonal and off-diagonal terms of the stiffness matrix (cf. Løken and Kaynia[27]). Notice that the stiffness matrix of the soil-monopile system used in the present study to extract the parameters in both AF approaches is derived from force-displacement curves obtained from FE simulations using Abaqus software. For more details on the determination of the FE-based stiffness matrix, the reader may refer to Jung et al.[20]

In this study, the terms of the stiffness matrix of the soil-monopile system were found to be $K_{HH} = 2.48 \times 10^9$ N/m for the lateral stiffness, $K_{RH} = 2.07 \times 10^{10}$ N/rad for the cross-coupling stiffness, and $K_{RR} = 4.12 \times 10^{11}$ N · m/rad for the rotational stiffness. Table 7 lists the parameters

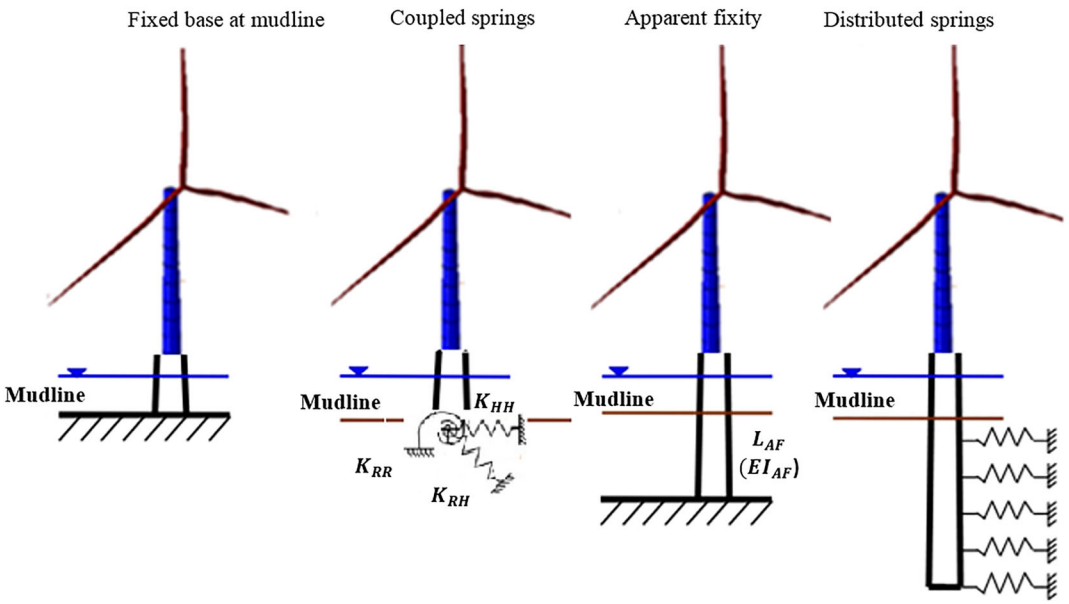

FIGURE 7 Alternative simplified foundation models analyzed in this paper

	K_{HH} (N/m)	K_{RR} (N · m/rad)	K_{RH} (N/rad)
Poulos and Davis[22]	2.40×10^{9}	2.43×10^{12}	7.20×10^{10}
Huggins and Basu[23]	2.55×10^{10}	3.49×10^{13}	8.70×10^{11}
Shadlou and Bhattacharya[24]	3.08×10^{10}	1.55×10^{13}	3.82×10^{11}

TABLE 6 Numerical values of the coupled springs

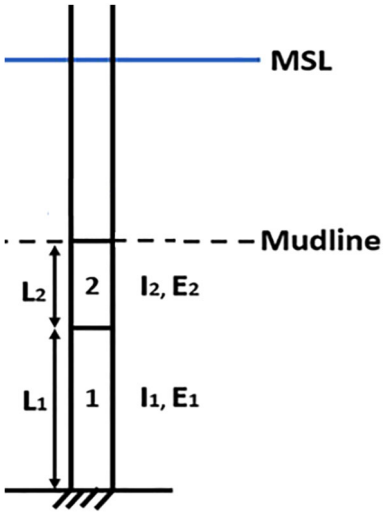

FIGURE 8 Improved apparent fixity AF method by Løken and Kaynia[27]

(length and stiffness) computed for both the traditional and improved AF approaches. In Table 7, it was assumed that the diameter and wall thickness of the two cylinders in the improved AF approach were kept the same as those of the monopile at mudline, i.e. 8.3 m and 0.09 m respectively, which implies that the area moment of inertia is the same for both cylinders (i.e. $I_1 = I_2 = I$). Also, a value of 5 m was assigned to the length L_2 of the upper cylinder. It should be noted here that a 3D representation was considered for the cylinder(s) used within the two AF approaches.

Concerning the distributed spring model considered in this section, it makes use of three different approaches to determine the distribution of the spring stiffness along the monopile embedded depth. The three approaches are based on the API $p - y$ curves (Equation 1), the modulus of subgrade reaction (Equation 2), and the CPT data (Equation 3). It should be noted that the API-based $p - y$ curves are derived based on the friction angle φ of the sand. In this study, this angle was calculated from the sand relative density D_r using the relationship given by Das and Sobhan[51] as follows:

TABLE 7 Computed values of the parameters of the traditional and improved AF approaches

	Traditional AF approach	Improved AF approach	
	Cylinder	Cylinder 1	Cylinder 2
Length L (m)	22.34	21.65	5
Flexural rigidity EI (N · m^2)	2.3×10^{12}	1.18×10^{13}	2.13×10^{12}

Abbreviation: AF, apparent fixity.

$$\varphi = 28^{\circ} + 0.18D_r. \tag{10}$$

Within the distributed spring model, a 3D representation of the monopile was adopted when implementing this approach in Abaqus. Notice however that the soil was modeled by 45 distributed spring elements [for each lateral (x or y) direction] equally spaced at 1.0 m interval along the monopile embedded length (of 45 m). This was done by creating 45 RPs that lie along the central vertical axis of the monopile. One end of each spring was connected to the corresponding RP, and the other end was fixed. Each RP was coupled to the corresponding monopile part (of 1 m depth).

Figure 9 shows the discrete spring stiffness distribution along the monopile embedded length (45 m) as given by the three approaches. Notice that the values of the spring stiffness in Figure 9 correspond to the initial stiffness (initial slope) of the p-y curves.

For each one of the nine simplified foundation models presented above, only the first natural frequency is reported herein for conciseness. Figure 10 shows a comparison between the first natural frequency obtained from the different foundation models and the one computed using the present 3D model. From Figure 10, one may observe that almost all of the foundation models considered in this study give an estimation of the first natural frequency which lies within the allowable frequency of the 10 MW DTU OWT (i.e. 0.176–0.273 Hz), except for the distributed spring model based on CPT data. It should be noted here that the 1P range for the 10 MW DTU corresponds to 0.1–0.16 Hz, while the 3P range corresponds to 0.3–0.48 Hz (cf. Bak et al.[36]). By considering a safety margin of 10%, the "allowable" frequency range for the OWT is thus 0.176–0.273 Hz.

Table 8 gives the percentage deviations between the values of the first natural frequency corresponding to the different simplified foundation models and that calculated using the developed 3D model. The CPT-based approach underestimates the natural frequency by about 14.9%

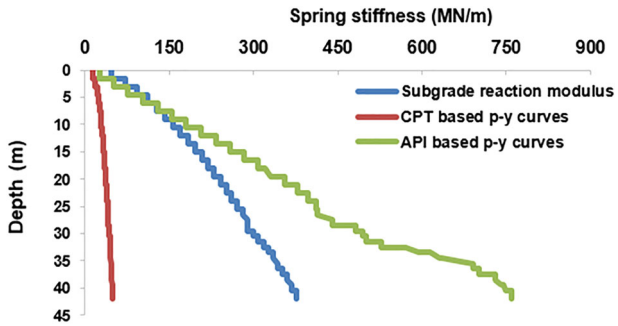

FIGURE 9 Spring stiffness distribution along the monopile embedded depth

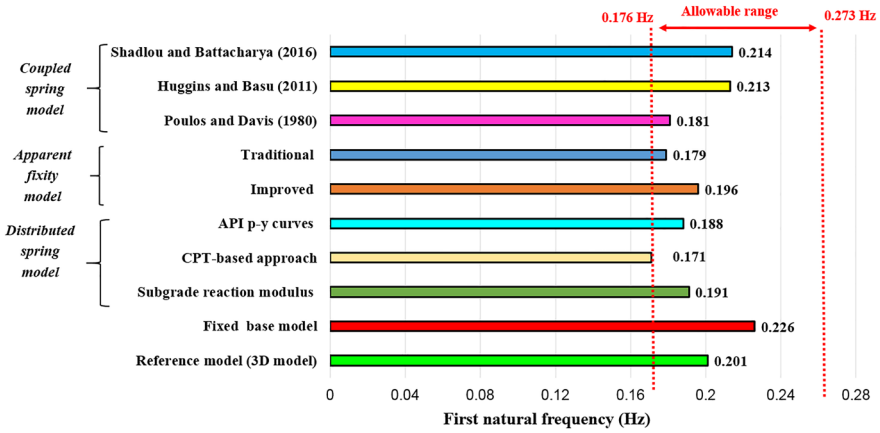

FIGURE 10 Predicted first natural frequency for several foundation models

TABLE 8 Deviation between the first natural frequency estimated using the 3D model and the ones estimated using the simplified foundation models

	Foundation models	1st natural frequency (Hz)	Deviation (%)
	3D model (reference model)	0.201	-
	Fixed-base model	0.226	12.4
Distributed springs model	Subgrade reaction modulus	0.191	−5
	CPT-based approach	0.171	−14.9
	API $p - y$ curves	0.188	−6.5
Apparent fixity model	Traditional	0.179	−10.9
	Improved	0.196	−2.5
Coupled springs model	Poulos and Davis[22]	0.181	−10
	Huggins and Basu[23]	0.213	6
	Shadlou and Bhattacharya[24]	0.214	6.5

compared to the 3D model. On the contrary, the fixed-base model overestimates the value of the frequency by around 12.4%, which is expected since the soil flexibility is neglected within this approach.

Concerning the coupled spring models, the expressions given by Poulos and Davis[22] underestimate the value of the natural frequency by 10%. However, both Huggins and Basu[23] and Shadlou and Bhattacharya[24] overestimate this frequency by about 6% and 6.5%, respectively. The values of the natural frequency calculated using the expressions provided by Huggins and Basu[23] and Shadlou and Bhattacharya[24] are close to the one obtained in the fixed-base model, thus overestimating the foundation stiffness.

Regarding the apparent fixity model, the traditional and improved AF approaches underestimate the value of the natural frequency by 10.9% and 2.5%, respectively. The big underestimation of the natural frequency by the traditional AF approach (10.9%) is due to the simplification adopted when calculating the AF model parameters by considering only the diagonal terms of the stiffness matrix and neglecting the off-diagonal terms. The result obtained by the improved AF approach proves the importance of considering the off-diagonal terms. This approach provides the best estimate of the natural frequency among all the simplified foundation models studied in this paper. It is important to note that the small relative deviation obtained with the improved AF approach is due to the fact that one makes use of the stiffness matrix obtained from the same FE model.

Notice finally that the distributed spring model based on the API $p - y$ curves and the one based on the modulus of subgrade reaction underestimate the natural frequency with a relatively acceptable deviation of 6.5% and 5%, respectively. The distributed spring model based on the modulus of subgrade reaction seems to come in the second place after the improved AF model, the subgrade reaction modulus being directly proportional to the small-strain Young modulus. This result is in conformity with the finding by Ashford and Juirnarongrit,[14] who concluded that models employing the modified expression of Vesic[15] for the modulus of subgrade reaction are capable of estimating the natural frequencies within a ratio of 0.98–1.04 times the measured experimental values.

Tuning of the simplified foundation models

This section investigates the accuracy of the natural frequency computed using the existing simplified soil-foundation models tuned on the 3D FEM-based model. This allows one to check the possibility of calibrating the existing simplified foundation models for an accurate characterization of the natural frequencies. The tuned foundation models used in this paper are the improved AF model, the coupled spring model, and the distributed spring model.

The tuning of the improved AF model based on the developed 3D model has been presented in the previous section, and it resulted in a very good estimate of the first natural frequency (with a deviation of 2.5%). It is important to mention that the calibration of the parameters of the improved AF model was done using the stiffness matrix of the 3D FEM-based model. Concerning the tuning of the coupled spring model, the stiffness of the coupled lateral and rotational springs (K_{HH}, K_{RR}, K_{RH}) correspond to the terms of the same stiffness matrix used to calibrate the parameters of the improved AF model. The value of the first natural frequency obtained using this tuned model (0.197 Hz) was found to be very close to the one obtained by the 3D developed model (0.201 Hz), the difference being smaller than 2%.

Finally, the tuning of the springs within the distributed spring model was obtained from FE simulations using Abaqus software. Notice that the springs stiffness distribution along the monopile embedded depth (of 45 m) were derived from the distribution of the lateral force and the corresponding lateral displacement shown in Figure 11. A total of 90 springs [for each lateral (x or y) direction] equally spaced at 0.5 m interval were considered to compute the natural frequency by the tuned model. The value of the first natural frequency obtained using this tuned model (0.196 Hz) was found to be very close to the one obtained by the 3D developed model (0.201 Hz), the difference being smaller than 2.5%.

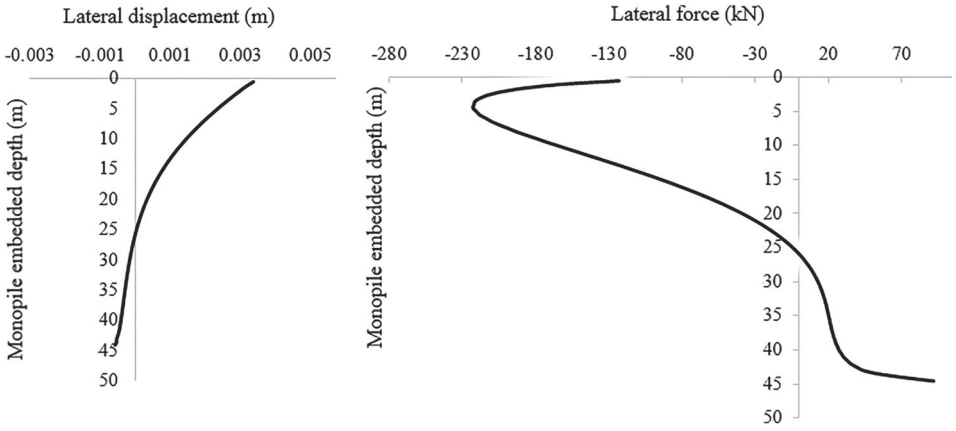

FIGURE 11 Lateral displacement distribution (left) and lateral force distribution (right) along the monopile embedded depth

4.3.2 | Superstructure models

The nacelle and rotor detailed modeling is not often a part of the FE models used by the majority of researchers in literature, where the RNA is poorly included in the analysis as a lumped mass placed at the top of the tower. Another frequent simplification used in literature is the modeling of the tower using beam elements. In order to investigate the suitability of the above-mentioned simplifications, three simplified superstructure models are considered, and their results are compared with those of the developed 3D FEM-based model. The three models labeled "Model 1," "Model 2," and "Model 3" are illustrated in Figure 12. All the three models consider a 3D soil domain as the developed 3D model. Model 1 replaces the RNA by a single lumped mass located at the top of the tapered tower; however, the tower is still modeled using shell elements. Model 2 consists in replacing (i) the tower by a tapered beam whose diameter and thickness of the different sections are decreasing from the bottom to the top of the tower and (ii) the RNA by a single lumped mass located at the tower top node. Model 3 consists in replacing the tower by an equivalent cylindrical beam with a constant diameter of 6.9 m (equal to the average tower diameter along its height) and a constant equivalent wall thickness of 2.95 cm. The equivalent thickness was computed such that the actual tower mass is maintained (cf. Arany et al.[19]). The RNA was considered in this model as a lumped mass located at the tower top. Notice finally that the properties of the lumped mass located at the tower top include the mass and the mass moments of inertia for the different directions. Table 9 lists the RNA data used in the three modeling approaches (cf. Bak et al.[36]).

Figure 13 and Table 10 show a comparison between the value of the first natural frequency obtained using the three simplified superstructure models and the one obtained by the present 3D model. From Figure 13 and Table 10, one may observe that the approximation made in Model 1 by the representation of the RNA as a lumped mass at the tower top tends to overestimate the first natural frequency by only 2.5%. The

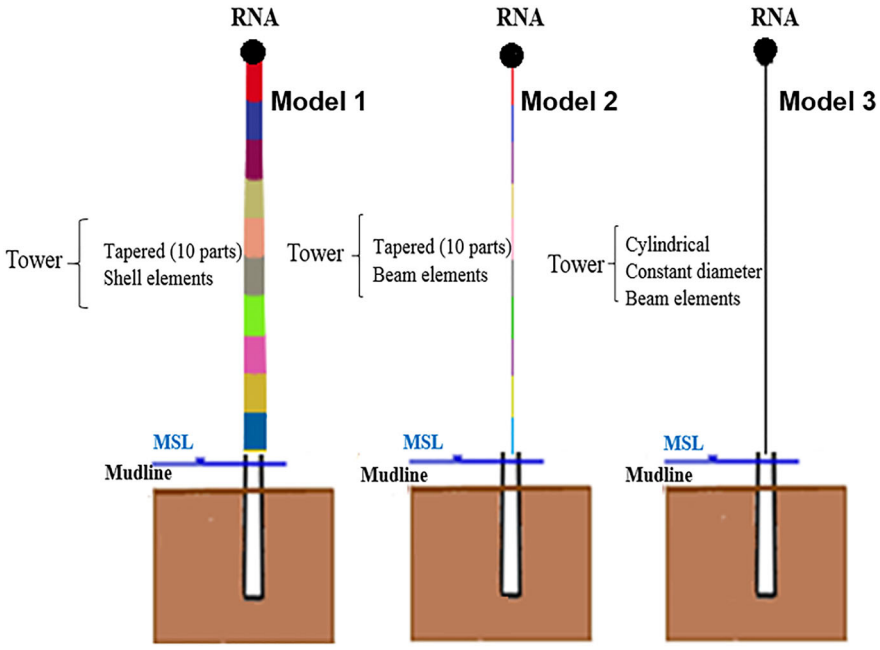

FIGURE 12 Simplified superstructure models analyzed in this paper

RNA at tower top	
Lumped mass (kg)	676,723
Moment of inertia about x-axis (kg · m^2)	1.66×10^8
Moment of inertia about y-axis (kg · m^2)	1.27×10^8
Moment of inertia about z-axis (kg · m^2)	1.27×10^8

TABLE 9 Rotor-nacelle-assembly data (cf. Bak et al.[36])

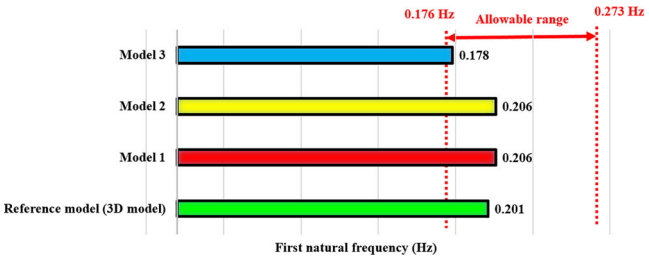

FIGURE 13 Predicted first natural frequency for several superstructure models

Superstructure models	1st natural frequency (Hz)	Deviation (%)
3D model (reference model)	0.201	-
Model 1	0.206	2.5
Model 2	0.206	2.5
Model 3	0.178	–11.4

TABLE 10 Deviation between the first natural frequency estimated using the 3D model and the ones estimated using the simplified superstructure models

same result was observed in Model 2 when the tower is modeled as a beam instead of shell elements. It should be noted here that Model 2 used the same thickness and diameter distribution (10 different parts along the tower height) for the tower as those used in Model 1, i.e. a tapered tower. Finally, the approximation made upon replacing the tapered tower by an equivalent cylinder with constant wall thickness and diameter (Model 3) underestimates the natural frequency by 11.4%.

5 | PARAMETRIC STUDY

A parametric study was performed using the developed 3D model to quantify the influence of the sand type, the monopile dimensions (diameter, thickness, and embedded depth), the water depth, and the transition piece (TP) height on the OWT first natural frequency.

Table 11 gives the first natural frequency of the DTU 10 MW OWT for a combination of values of the water depth, the monopile geometric properties (outer diameter, wall thickness), and the type of sand. Figure 14 gives a graphical representation of the data given in Table 11 for the case of very dense sand. It should be noted that the results shown in Table 11 and Figure 14 were calculated for a constant monopile embedded depth of 45 m. From Table 11 and Figure 14, one may observe that the first natural frequency of the OWT increases with the increase of the monopile outer diameter. For instance, the first natural frequency increases by around 8.4% as the monopile diameter increases from 8.3 m (with 9 cm thickness) to 10 m (with 11 cm thickness) in the case of the 10 MW OWT installed in a loose sand at a water depth of 25 m. A rise in the natural frequency was also observed with the increase of the monopile wall thickness and the decrease of the water depth. For instance, the reduction in the water depth from 45 to 25 m leads to an augmentation in the natural frequency by about 10.9% for a monopile diameter/wall thickness of 8.3 m/9 cm embedded in a loose sand. Furthermore, the rise in the soil density (change from loose to medium dense or very dense sand) results in an increase in the first natural frequency. This augmentation is equal to 0.64% and 1.2% only as the soil type passes from loose to medium dense and from loose to very dense sand respectively for a monopile diameter/wall thickness of 8.3 m/9 cm and a water depth of 25 m. It can be seen from the obtained results that the type of sand does not induce a significant change in the first natural frequency.

Figure 15 illustrates the effect of varying the monopile embedment depth L (from 1D to 12D) on the first natural frequency of the DTU 10 MW OWT for two monopile diameters D (D = 8.3 and 10 m) and for two sand types (loose and very dense sands). It should be noted that the results shown in Figure 15 were calculated for a constant water depth of 25 m. From Figure 15, one may observe that increasing the embedment depth from 5D to 12D has no significant influence on the first natural frequency of the OWT having a designed pile diameter of 8.3 m and installed in loose or very dense sand. A decrease in the embedment depth below 5D significantly reduces the natural frequency. For a higher diameter of 10 m, it may be observed that the natural frequency reaches a plateau for an embedded depth of 4D when installed in loose sand and

TABLE 11 Values of the first natural frequency for different values of water depth, monopile diameter, and thickness and for three types of sand at a constant monopile embedded depth of 45 m

			Natural frequency (Hz)		
Water depth (m)	Monopile outer diameter (m)	Thickness (cm)	Loose sand	Medium dense sand	Very dense sand
25	8.3	9	0.2009	0.2022	0.2034
		10	0.2020	0.2035	0.2045
		12	0.2056	0.2070	0.2082
	9	10	0.2074	0.2087	0.2100
		12	0.2112	0.2125	0.2136
		14	0.2158	0.2169	0.2178
	10	11	0.2177	0.2187	0.2196
		13	0.2186	0.2197	0.2206
		15	0.2207	0.2217	0.2226
35	8.3	9	0.1909	0.1923	0.1935
		10	0.1928	0.1941	0.1953
		12	0.1970	0.1984	0.1997
	9	10	0.1992	0.2006	0.2018
		12	0.2038	0.2051	0.2063
		14	0.2092	0.2103	0.2113
	10	11	0.2096	0.2108	0.2119
		13	0.2129	0.2141	0.2151
		15	0.2155	0.2166	0.2176
45	8.3	9	0.1811	0.1825	0.1837
		10	0.1836	0.1850	0.1861
		12	0.1890	0.1902	0.1907
	9	10	0.1909	0.1922	0.1935
		12	0.1962	0.1976	0.1988
		14	0.2023	0.2035	0.2045
	10	11	0.2030	0.2042	0.2054
		13	0.2070	0.2082	0.2092
		15	0.2101	0.2113	0.2123

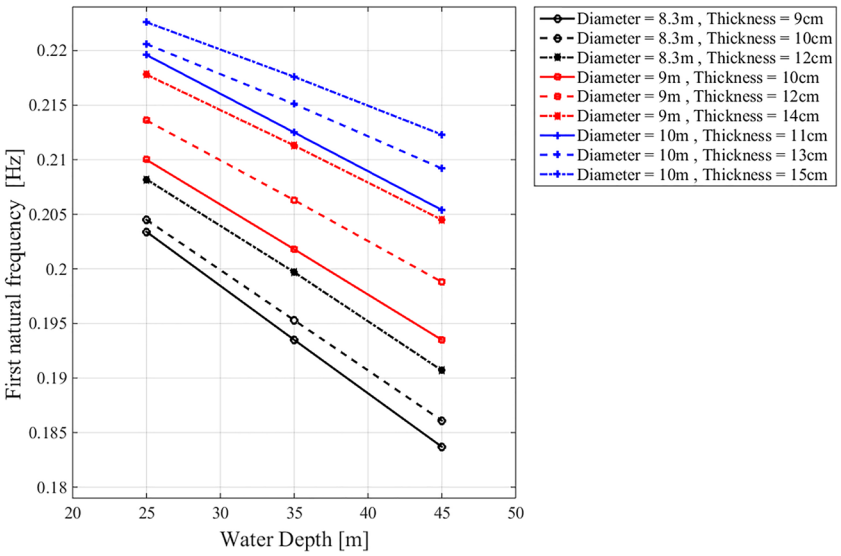

FIGURE 14 First natural frequency variation as a function of the water depth (m), the monopile diameter, and thickness for the case of a very dense sand. This figure is a graphical representation of the data given in Table 11

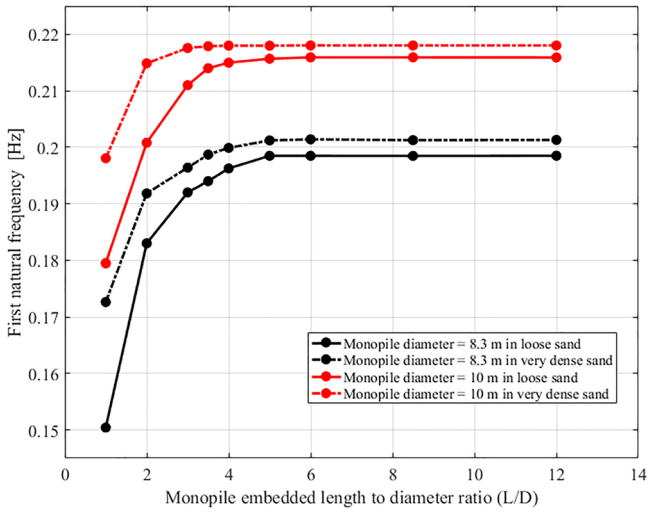

FIGURE 15 First natural frequency versus the monopile embedded length for two monopile diameters and installed in two sand types at a water depth of 25 m

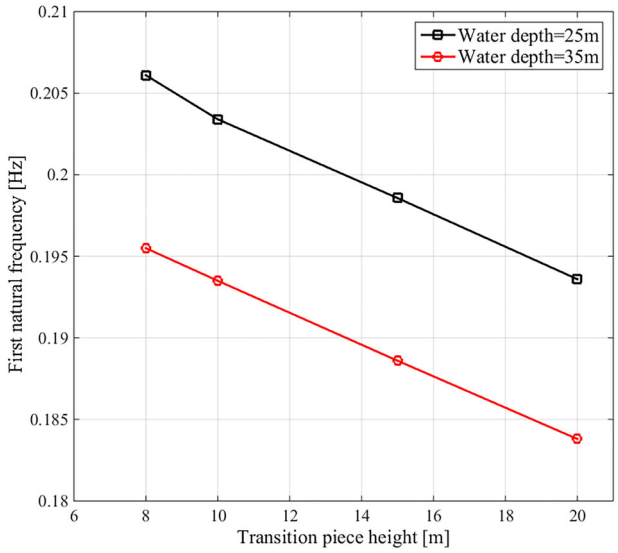

FIGURE 16 First natural frequency versus the transition piece height (m) at two different water depths in the case of a very dense sand. The transition piece diameter and thickness are kept constant (8.3 m and 9 cm, respectively)

3.5D when installed in very dense sand. The observed behavior related to the stabilization of the first natural frequency was previously reported by Senanayake et al.[52] when modeling the soil-monopile interaction using the distributed spring model. It may be explained by the fact that the structure becomes more rigid due to the increase of the clamped zone in the soil. Finally, notice that the increase in the monopile diameter from 8.3 to 10 m (for a monopile embedded length beyond the critical one) is shown to induce a significant increase by about 8.8% in the value of the first natural frequency in the case of a loose sand.

In addition to the above-mentioned parameters, the transition piece design parameters (i.e. diameter, thickness, and height) may influence the vibration frequencies of the structure. In this paper, the TP diameter and thickness are kept identical to those of the tower and foundation to ensure a continuous profile. Figure 16 gives the first natural frequency of the DTU 10 MW OWT for four different TP heights (8, 10, 15, and 20 m) at two different water depths (25 and 35 m). It should be noted that the results shown in Figure 16 were calculated for the case of an OWT installed in very dense sand and for a monopile diameter/thickness of 8.3 m/9 cm. From Figure 16, one may observe that the first natural frequency of the OWT decreases with the increase of the TP height. For instance, the first natural frequency decreases by about 6% as the TP height increases from 8 to 20 m for both values of water depth of 25 and 35 m.

6 | CONCLUSIONS

In this paper, a 3D model that explicitly considers the geometrical properties of the whole OWT superstructure (blades, tower, and transition piece) and the 3D soil domain together with its interaction with the monopile foundation was developed. The aim was to accurately compute the natural frequencies of the 10 MW DTU OWT installed in sand in the scope of investigating the suitability of the different simplified models

(for the soil-foundation system and the superstructure) found in literature when calculating the natural frequencies. The results obtained from this investigation provide practicing engineers who use simplified models how poorly the models they use are when predicting the natural frequencies.

A comparison between the results obtained from the developed 3D model and those corresponding to the mostly used simplified foundation and superstructure models was performed. A tuning of the simplified foundation models was also investigated making use of the developed 3D model to give insight about the possibility of calibrating the simplified foundation models to be used in time-domain aero-elastic simulations. Finally, the influence of the water depth, the sand relative density, the monopile geometrical properties (diameter, thickness, and embedded depth), and the transition piece height on the first natural frequency was investigated. Based on the obtained numerical results, the following conclusions may be drawn:

1. The first bending modes of the tower in the side-side and the fore-aft directions are the major mode shapes of a monopile-supported OWT.
2. The refined modeling of the grouted connection does not have a significant effect on the first system natural frequency.
3. The first vibration frequency of the tower is significantly decreased (by 11.1%) when the SSI is considered.
4. Among the different foundation models found in literature, the improved apparent fixity approach by Løken and Kaynia[27] (which was tuned based on the 3D FEM-based model) resulted in the best estimate of the first natural frequency with a deviation of around 2.5%. This small difference is due to the fact that the stiffness matrix is obtained from the same FE model. The distributed spring model based on the modulus of subgrade reaction comes in the second place. It gives the best estimate compared to the other distributed spring models with a deviation of around 5%.
5. The tuning of the different simplified foundation models (coupled springs, improved apparent fixity, and the distributed spring model) based on the 3D FEM-based model proved to give a very good estimate of the first natural frequency with a maximal deviation of about 2.5%.
6. The results obtained from the simplified superstructure models proved that the representation of the RNA by a lumped mass with the corresponding mass and moment of inertia properties gives an estimation of the first natural frequency with a deviation of 2.5% only. Moreover, the assumption of modeling the tower with 3D shell elements does not improve the results significantly, and thus, the assumption of using a tapered beam with the corresponding geometrical and mass properties is sufficient when calculating the first natural frequency.
7. The natural frequency of the OWT increases with an increase in the monopile outer diameter and wall thickness. This can be explained by the increase in the stiffness of the foundation. The increase of the soil relative density results in a very small increase in the first natural frequency (of about 1.2% when the soil type changes from loose sand to a very dense sand).
8. The first natural frequency of the OWT increases with an increase in the monopile embedded length, and then it becomes constant beyond a critical embedded depth as was reported by Senanayake et al.[52] The limit value of the embedded depth reduces with the rise in the monopile diameter and the sand relative density. The finding related to the critical embedded depth is important in design in order to avoid unnecessary over length of the monopile embedded depth.

ACKNOWLEDGEMENTS

This work is carried out within the framework of the West Atlantic Marine Energy Community (WEAMEC) and the funding from the Communauté d'Agglomération de la Région Nazairienne et de l'Estuaire (CARENE). The authors would like to thank the four anonymous reviewers for their insightful suggestions that largely contributed in improving the manuscript.

PEER REVIEW

The peer review history for this article is available at https://publons.com/publon/10.1002/we.2598.

ORCID

Philip Alkhoury https://orcid.org/0000-0002-4294-3870
Abdul-Hamid Soubra https://orcid.org/0000-0002-4596-5979
Valentine Rey https://orcid.org/0000-0003-1019-1819
Mourad Aït-Ahmed https://orcid.org/0000-0003-3633-4275

REFERENCES

1. Zaaijer MB. Foundation modelling to assess dynamic behaviour of offshore wind turbines. *Appl Ocean Res*. 2006;28(1):45-57.
2. Bazeos N, Hatzigeorgiou GD, Hondros ID, Karamaneas H, Karabalis DL, Beskos DE. Static, seismic and stability analyses of a prototype wind turbine steel tower. *Eng Struct*. 2002;24:1015-1025.
3. Lavassas I, Nikolaidis G, Zervas P, Efthimiou E, Doudoumis IN, Baniotopoulos CC. Analysis and design of the prototype of a steel 1-MW wind turbine tower. *Eng Struct*. 2003;25(8):1097-1106.
4. Asareh M, Schonberg W, Volz J. Fragility analysis of 5 MW NREL wind turbine considering aero-elastic and seismic interaction using finite element method. *Finite Elements in Analysis and Design*. 2016;120:57-67.

5. Winkler E. Die lehre von elastizitat and festigkeit (on elasticity and fixity). Prague; 1867.
6. American Petroleum Institute (API). Petroleum and natural gas industries-specific requirement for offshore structures. Part 4—Geotechnical and foundation design considerations. 2011.
7. Andersen LV, Vahdatirad MJ, Sichani MT, Sørensen JD. Natural frequencies of wind turbines on monopile foundations in clayey soils—a probabilistic approach. *Comput Geotech*. 2012;43:1-11.
8. Bisoi S, Haldar S. Dynamic analysis of offshore wind turbine in clay considering soil-monopile-tower interaction. *Soil Dyn Earthq Eng*. 2014;63:19-35.
9. Haldar S, Sharma J, Basu D. Probabilistic analysis of monopile-supported offshore wind turbine in clay. *Soil Dyn Earthq Eng*. 2018;105:171-183.
10. Wang P, Zhao M, Du X, Liu J, Xu C. Wind, wave and earthquake responses of offshore wind turbine on monopile foundation in clay. *Soil Dyn Earthq Eng*. 2018;113:47-57.
11. Zuo H, Bi K, Hao H. Dynamic analyses of operating offshore wind turbines including soil-structure interaction. *Eng Struct*. 2018;157:42-62.
12. Prendergast LJ, Gavin K, Doherty P. An investigation into the effect of scour on the natural frequency of an offshore wind turbine. *Ocean Eng*. 2015;101:1-11.
13. Prendergast LJ, Reale C, Gavin K. Probabilistic examination of the change in eigenfrequencies of an offshore wind turbine under progressive scour incorporating soil spatial variability. *Mar Struct*. 2018;57:87-104.
14. Ashford S, Juirnarongrit T. Evaluation of pile diameter effect on initial modulus of subgrade reaction. *J Geotech Geoenvironmental Eng*. 2013;129:234-242.
15. Vesic A. Bending of beams resting on isotropic elastic solid. *J Soil Mech Found Div*. 1961;87:35-53.
16. Suryasentana S, Lehane B. Numerical derivation of CPT-based p-y curves for piles in sand. *Géotechnique*. 2014;64(3):186-194.
17. Adhikari S, Bhattacharya S. Vibrations of wind-turbines considering soil-structure interaction. *Wind Struct*. 2011;14(2):85-112.
18. Arany L, Bhattacharya S, Adhikari S, Hogan SJ, Macdonald JHG. An analytical model to predict the natural frequency of offshore wind turbines on three-spring flexible foundations using two different beam models. *Soil Dyn Earthq Eng*. 2015;74:40-45.
19. Arany L, Bhattacharya S, Macdonald JHG, Hogan SJ. Closed form solution of eigen frequency of monopile supported offshore wind turbines in deeper waters incorporating stiffness of substructure and SSI. *Soil Dyn Earthq Eng*. 2016;83:18-32.
20. Jung S, Kim SR, Patil A, Hung LC. Effect of monopile foundation modeling on the structural response of a 5-MW offshore wind turbine tower. *Ocean Eng*. 2015;109:479-488.
21. Jonkman JM, Buhl M. FAST user's guide, technical report, August 2005.
22. Poulos HG, Davis EH. *Pile Foundation Analysis and Design*. New York: Rainbow-Bridge Book., Wiley; 1980.
23. Huggins W, Basu D. *Fourier Finite Element Analysis of Laterally Loaded Piles in Elastic Media*. Connecticut, US: Storrs; 2011.
24. Shadlou M, Bhattacharya S. Dynamic stiffness of monopiles supporting offshore wind turbine generators. *Soil Dyn Earthq Eng*. 2016;88:15-32.
25. Abhinav KA, Saha N. Dynamic analysis of monopile supported offshore wind turbines. *Proc Inst Civ Eng Geotech Eng*. 2017;170(5):428-444.
26. Velarde J, Vanem E, Kramhøft C, Sørensen JD. Probabilistic analysis of offshore wind turbines under extreme resonant response: application of environmental contour method. *Appl Ocean Res*. 2019;93:1-16, 101947.
27. Løken IB, Kaynia AM. Effect of foundation type and modelling on dynamic response and fatigue of offshore wind turbines. *Wind Energy*. 2019;22(12):1667-1683.
28. Achmus M, Thieken K. On the behaviour of piles in non-cohesive soil under combined horizontal and vertical loading. *Acta Geotech*. 2010;5:199-210.
29. Abdel-Rahman K, Achmus M. Finite element modelling of horizontally loaded monopile foundations for offshore wind energy converters in Germany. In: *Proceedings of the International Symposium on Frontiers in Offshore Geotechnics*. Perth: Taylor and Francis; 2005:391-396.
30. Prowell I. An experimental and numerical study of wind turbines seismic behabviour. [Dissertation of PhD]. San Diego: University of California: 2011.
31. Jalbi S, Bhattacharya S. A comparison between advanced and simplified methods to predict the natural frequency of offshore wind turbines incorporating soil-structure interaction. *Coastal Structures, Goseberg, Nils & Schlurmann, Torsten: Karlsruhe: Bundesanstalt fur Wasserbau*. 2019;904-912.
32. Corciulo S, Zanoli O, Pisano F. Transient response of offshore wind turbines on monopiles in sand: role of cyclic hydro-mechanical soil behaviour. *Comput Geotech*. 2017;83:221-238.
33. Kementzetzidis E, Versteijlen WG, Nernheim A, Pisano F. 3D FE dynamic modelling of offshore wind turbines in sand: natural frequency evolution in the pre- to after-storm transition. In: Proceedings of the 9th European Conference on Numerical Methods in Geotechnical Engeneering (NUMGE 2018), Porto, Portugal; 2018.
34. Kementzetzidis E, Corciulo S, Versteijlen WG, Pisano F. Geotechnical aspects of offshore wind turbine dynamics from 3D non-linear soil-structure simulations. *Soil Dyn Earthq Eng*. 2019;120:181-199.
35. Ma H, Yang J, Chen L. Numerical analysis of the long-term performance of offshore wind turbines supported by monopiles. *Ocean Eng*. 2017;136:94-105.
36. Bak C, Zahle F, Bitsche R, Kim T, Yde A, Henriksen LC, Hansen MH, Blasques JPAA; Gaunaa M, Natarajan A. Description of the DTU 10 MW reference wind turbine. DTU Wind energy report-I-0092. 2013;(July):1–138. https://dtu-10mw-rwt.vindenergi.dtu.dk
37. API RAW. Recommended practice for planning, designing and constructing fixed offshore platforms-working stress design. API RP2A-WSD. 2000.
38. Letcher TM. Wind energy engineering: A handbook for onshore and offshore wind turbines.; 2017.
39. Bi K, Hao H. Using pipe-in-pipe systems for subsea pipeline vibration control. *Eng Struct*. 2016;109:75-84.
40. Gentils T, Wang L, Kolios A. Integrated structural optimisation of offshore wind turbine support structures based on finite element analysis and genetic algorithm. *Appl Energy*. 2017;199:187-204.
41. CFMS Comité Français de Mécanique des Sols et de Géotechnique. Recommendations for planning and designing foundations of offshore wind turbines 2015.
42. Hardin BO, Black WL. Sand stiffness under various triaxial stresses. *J Soil Mech Found Div*. 1996;92(2):27-42.
43. Seed H, Idriss I. Soil moduli and damping factors for dynamic response analyses. Report EERC 70-10, Earthquake Engineering Research Center, University of California, Berkeley, 1970.
44. Hardin BO, Drnevich VP. Shear modulus and damping in soils: design equations and curves. *Soil Mech Found Div*. 1972;98(SM7):667-692.
45. Jardine R. ICP design methods for driven piles in sands and clays. 2015.
46. Oztoprak S, Bolton M. Stiffness of sands through laboratory test database. *Géotechnique*. 2013;63:54-70.

47. Lunne T, Christopherson H. Interpenetration of cone penetrometer data for offshore sands. In: Proceedings of the Offshore Technology Conference OTC4464. Houston, Texas. 1983.
48. Gu X, Yang J, Huang M. Laboratory measurements of small strain properties of dry sands by bender element. *Soils Found*. 2013;53(5):735-745.
49. Larsen TJ, Hansen AM. How 2 HAWC2, the user's manual, 2007.
50. Densit. n.d., Ducorit data sheet-ultra high performance grout.
51. Das BM, Sobhan K. Principles of geotechnical engineering, 2016.
52. Senanayake A, Gilbert RB, Manuel L. Estimating natural frequencies of monopile supported wind turbines using alternative p-y models. Offshore Technology Conference, 2017.

How to cite this article: Alkhoury P, Soubra A-H, Rey V, Aït-Ahmed M. A full three-dimensional model for the estimation of the natural frequencies of an offshore wind turbine in sand. *Wind Energy*. 2020;1–21. https://doi.org/10.1002/we.2598